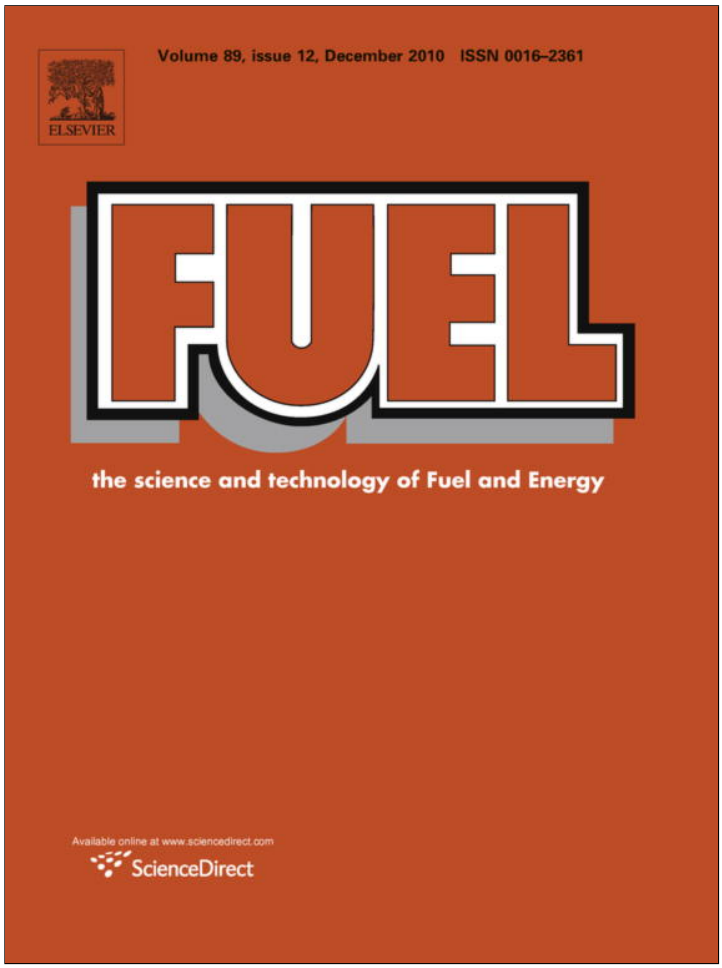

Fuel 89 (2010) 4014–4024

Contents lists available at ScienceDirect

Fuel

journal homepage: www.elsevier.com/locate/fuel

# A comparison of injector flow and spray characteristics of biodiesel with petrodiesel

S. Som [a,*], D.E. Longman [a], A.I. Ramírez [b], S.K. Aggarwal [b]

[a] Argonne National Laboratory, 9700 S. Cass Avenue, Argonne, IL 60439, USA
[b] Department of Mechanical and Industrial Engineering, University of Illinois at Chicago, Chicago, IL 60607, USA

ARTICLE INFO

*Article history:*
Received 4 March 2010
Received in revised form 26 April 2010
Accepted 9 May 2010
Available online 20 May 2010

*Keywords:*
Biodiesel
Diesel
Primary breakup
Cavitation
Spray

ABSTRACT

Performance and emission characteristics of compression ignition engines depend strongly on inner nozzle flow and spray behavior. These processes control the fuel air mixing, which in turn is critical for the combustion process. The differences in the physical properties of petrodiesel and biodiesel are expected to significantly alter the inner nozzle flow and spray structure and, thus, the performance and emission characteristics of the engine. In this study, the inner nozzle flow dynamics of these fuels are characterized by using the mixture-based cavitation model in FLUENT v6.3. Because of its lower vapor pressure, biodiesel was observed to cavitate less than petrodiesel. Higher viscosity of biodiesel resulted in loss of flow efficiency and reduction in injection velocity. Turbulence levels at the nozzle orifice exit were also lower for biodiesel. Using the recently developed KH-ACT model, which incorporates the effects of cavitation and turbulence in addition to aerodynamic breakup, the inner nozzle flow simulations are coupled with the spray simulations in a "quasi-dynamic" fashion. Thus, the influence of inner nozzle flow differences on spray development of these fuels could be captured, in addition to the effects of their physical properties. Spray penetration was marginally higher for biodiesel, while cone angle was lower, which was attributed to its poor atomization characteristics. The computed liquid lengths of petrodiesel and biodiesel were compared with data from Sandia National Laboratories. Liquid lengths were higher for biodiesel due to its higher boiling temperature and heat of vaporization. Though the simulations captured this trend well, the liquid lengths were underpredicted, which was attributed to uncertainty about the properties of biodiesel used in the experiments. Parametric studies were performed to determine a single parameter that could be used to account for the observed differences in the fuel injection and spray behavior of petrodiesel and biodiesel; fuel temperature seems to be the best parameter to tune.



## 1. Introduction

Concerns about energy security and environment have stimulated worldwide interest in biologically derived alternative fuels. Biodiesel presents a lucrative alternative, particularly for compression ignition engines, because it is a renewable energy source that can be used in these engines without significant changes in their design. Modern diesel engines can operate with 5–10% addition of biodiesel by volume without any loss in performance. Thus, even using biodiesel as an additive can prolong the use of petrodiesel. Biodiesel can be produced from a variety of feedstocks, generally through the transesterification process using an alcohol. Being an oxygenated fuel, it is environmentally cleaner than petrodiesel (aka "diesel") with respect to unburnt hydrocarbon (UHC) and particulate matter (PM) emissions.

Graboski and McCormick [1] reported an excellent review of the physical properties of petrodiesel and biodiesel. They concluded that biodiesel is completely miscible with petrodiesel and enhances its lubricity. There have been several studies on the combustion and emissions characteristics of biodiesel and bio-/petrodiesel blends [1–5], but those dealing with their injection, atomization, and spray behavior are sparse, especially from a computational fluid dynamics (CFD) standpoint. Miers et al. [6] studied the rate of injection characteristics of these fuels and found that injected volume for biodiesel was lower due to its higher viscosity compared to diesel. The amount of injected energy was also lower, since the heat of combustion of biodiesel is about 10% lower than that of petrodiesel [1]. Suh et al. [7], performing experiments to examine the inner nozzle flow characteristics of petrodiesel and biodiesel for a scaled-up nozzle, and found that injection velocity and mass flow rate were lower for biodiesel, again due to its higher viscosity. Park et al. [8] observed the Sauter mean diameter to be higher for biodiesel, indicating poor atomization compared to petrodiesel.

Using X-ray radiography, Kastengren et al. [9] examined the near nozzle structure of non-evaporating viscor (a diesel

* Corresponding author. Address: Argonne National Laboratory, Energy Systems Division, 9700 S. Cass Avenue, Argonne, IL 60439, USA. Tel.: +1 630 252 5273; fax: +1 630 252 3443.
*E-mail address:* ssom@anl.gov (S. Som).

0016-2361/$ - see front matter © 2010 Elsevier Ltd. All rights reserved.
doi:10.1016/j.fuel.2010.05.004

calibration fluid) spray and a biodiesel–viscor blend spray. In general, the spray structures for these fuels were similar, with biodiesel showing marginally smaller cone angle. Grimaldi and co-workers [3,10,11] performed experiments to compare the spray characteristics of biodiesel and petrodiesel for cylindrical and conical nozzles. Diesel fuel exhibited significant differences in penetration and cone angle in going from the cylindrical to the conical nozzle. However, with biodiesel the differences in spray structure and penetration were small for the two nozzles. In addition, the biodiesel spray penetrated more and spread less compared with diesel fuel. While no cavitation or turbulence measurements were performed, these differences were attributed to the expected differences in cavitation characteristics. Higgins et al. [12] measured the maximum liquid penetration for different fuels, including diesel, biodiesel, methanol, gasoline, and *n*-hexadecane. They found that the liquid length for biodiesel was higher than that for diesel, which they attributed to biodiesel's higher boiling temperature and heat of vaporization.

Chakravarthy et al. [13] reported a comparison of the physical properties of petrodiesel and biodiesel as a function of temperature, observing that the density, surface tension, and kinematic viscosity of biodiesel are higher than those of diesel, whereas the vapor pressure and heat capacity are lower. These differences in physical properties are expected to have a significant influence on their spray and combustion characteristics [14].

Diesel engine simulations have also been performed using biodiesel fuel. Brakora et al. [15] developed a reduced mechanism using methyl butanoate as a surrogate for biodiesel, which consisted of 41 species and 150 elementary reactions. In performing engine simulations using KIVA/CHEMKIN, they assumed that the injection characteristics are similar for these fuels, which may not be an accurate assumption. However, the mechanism successfully predicted ignition timing, pressure, heat release rate, and emission characteristics. Using the same biodiesel surrogate, Ra et al. [16] performed parametric studies to investigate the effects of various physical properties on combustion characteristics; they observed that the results were most sensitive to liquid density, vapor pressure, and surface tension.

The literature search identified relatively few studies dealing with the injection and spray characteristics of biodiesel fuels. Since there are significant differences in the thermo-transport properties of petrodiesel and biodiesel fuels, the injection and spray characteristics of biodiesel can be expected to differ from those of petrodiesel. For instance, due to differences in vapor pressure, surface tension, and viscosity, the cavitation and turbulence characteristics of biodiesel and diesel fuels inside the injector may be significantly different. The injector flow characteristics determine boundary conditions at the injector orifice exit, including the rate of injection (ROI) profile as well as the cavitation and turbulence levels; this can have a significant influence on the atomization and spray characteristics, and consequently on engine performance. This provides the major motivation for the present study.

The major objective of the present study is to quantify differences, using a detailed computational model, between the injection and spray characteristics of biodiesel and diesel fuels. Simulations were first performed to investigate the effects of thermo-transport properties of biodiesel and diesel fuels on the inner nozzle flow characteristics, including the amount of cavitation and turbulence at the injector exit. A parametric study was also performed to examine the necessary changes in the injection and ambient conditions so that there would be no loss of flow efficiency while injecting biodiesel. Then a detailed two-phase model in an engine modeling software, CONVERGE [17–19], was employed to examine the atomization and spray characteristics of diesel and biodiesel fuels under diesel engine conditions. These characteristics include spray penetration, dispersion, liquid length, Sauter mean diameter, cone angle, and liquid density and vapor mass fraction distribution. The effect of inner nozzle flow on the atomization and spray behavior of the two fuels was also investigated by "quasi-dynamically" coupling the injector flow and spray simulations. The coupling was achieved by using a recently developed primary breakup model, KH-ACT (Kelvin Helmholtz-*A*erodynamic *C*avitation *T*urbulence), which captures the effects of cavitation and turbulence on primary liquid breakup, in addition to aerodynamic breakup [20–23]. In this context, it is important to mention that in a recent study [24], it was observed that, compared to the commonly used KH-based primary breakup model, the KH-ACT model provides better predictions for atomization and spray behavior, since the latter model captures the effects of cavitation and turbulence generated inside the injector. Therefore, another objective of the present study was to further validate the KH-ACT model and establish the importance of capturing the effects of inner nozzle flow on the primary breakup, in order to accurately predict the spray characteristics of biodiesel and diesel fuels.

## 2. Computational-physical model

The inner nozzle flow simulations were performed using the CFD software FLUENT v6.3 [25], while the two-phase flow simulations for the atomization and spray behavior of biodiesel and diesel fuels were performed using the Eulerian–Lagrangian CFD software CONVERGE [17–19,23]. These two sets of simulations were "quasi-dynamically" coupled (i.e., the boundary conditions at the injector orifice exit were obtained from inner nozzle flow simulations). A brief description of the physical-numerical models for the two simulations is provided below.

### 2.1. Injector flow simulations

The CFD software FLUENT v6.3 employs a mixture-based approach [26,27]; a mixture comprising liquid fuel, vapor, and a non-condensable gas is considered. A no-slip condition between the liquid and vapor phases is assumed. The mixture properties are computed by using the Reynolds-Averaged continuity and momentum equations [25]. In order to account for large pressure gradients, the RNG $k-\in$ turbulence model is incorporated along with the non-equilibrium wall functions. Vapor generation and condensation are calculated by using the simplified solution of the Rayleigh–Plesset equation [28]. Further details of the physical model and governing equations can be found in Singhal et al. [27] and Som et al. [23,26].

A full-production mini-sac nozzle used in the present study is shown in Fig. 1. The nozzle has six cylindrical holes, each

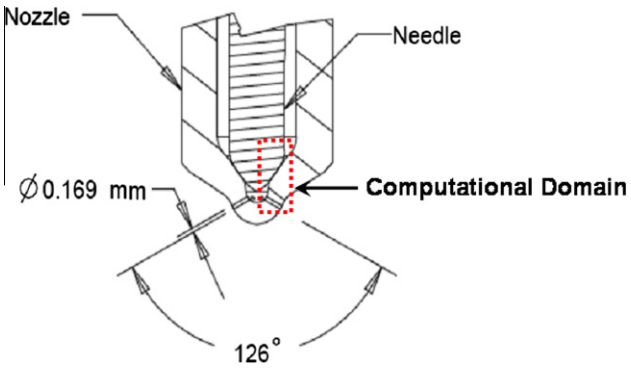


**Fig. 1.** Schematic of six-hole full-production mini-sac nozzle. Only two holes are seen in this cross-sectional slice. Nozzle and needle region are identified along with the computational zone used in simulations. The orifice diameter is 169 μm with an included angle of 126°.

169 μm in diameter, at an included angle of 126°. The flow is assumed to be symmetric across all the nozzle orifices, so only a single orifice is simulated; the computational domain (single orifice) used in the simulations is indicated by a marked box. Fig. 2 shows front and back views of the three-dimensional 60°-sector mesh generated. The sac region is characterized by tetrahedral elements, while other zones consist of structured orthogonal grids. To ensure grid independence [23,26], a total of 60,000 cells were generated. The pressure values are specified at the inlet and outlet boundaries, while symmetry conditions are employed to demarcate the 60°-sector mesh. All the other surfaces are specified as wall boundaries, with no slip between the fuel–air mixture and nozzle orifice walls. In order to facilitate the "quasi-dynamic" coupling, steady-state, three-dimensional (3-D) nozzle flow simulations were performed at five different needle-lift positions – namely, 0.05, 0.1, 0.15, 0.2, and 0.275 mm (peak needle-lift position). Parameters (such as injection velocity, cavitation, and turbulence levels) required for spray simulations were calculated for each needle-lift position or duration of injection (cf. Fig. 9). Simulations were performed at a fixed back pressure of 30 bar; the injection pressure ranged from 800 to 1600 bar, depending upon the needle-lift position.

### 2.2. Spray simulations

Fuel atomization and spray simulations were performed using the Eulerian–Lagrangian approach in the CFD software CONVERGE [17–19,23]. It incorporates state-of-the-art models for spray injection, atomization and breakup, turbulence, droplet collision, and coalescence. The details of these models can be found in previous publications, so only a brief description is provided here.

CONVERGE uses an innovative, modified cut-cell Cartesian method for grid generation [17–19]. The grid is generated internally to the code at runtime. For all cases, the base grid size was fixed at 4 mm. In order to resolve the flow near the injector, a fixed grid embedding is employed such that the minimum grid size is 0.5 mm. Apart from this region, it is rather difficult to determine *a priori* where a refined grid is needed. Hence, three levels of adaptive mesh refinement are employed for the velocity field, such that the minimum grid size is 0.5 mm. In order to match the spray chamber geometry used in the experimental study [12], a cylindrical geometry of 100 mm in diameter and 100 mm in length is generated for evaporating sprays. Similarly, in order to match the geometry used for X-ray experiments at Argonne [23,24], a cylindrical geometry of 50 mm in diameter and 200 mm in length is generated for non-evaporating sprays.

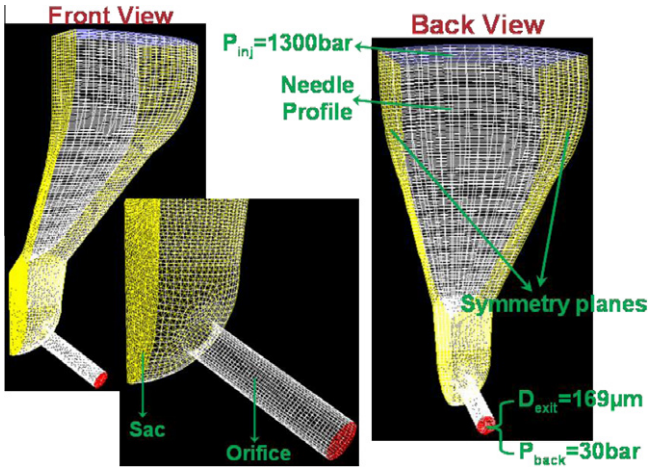


**Fig. 2.** Three-dimensional grid generated for inner nozzle flow simulations.

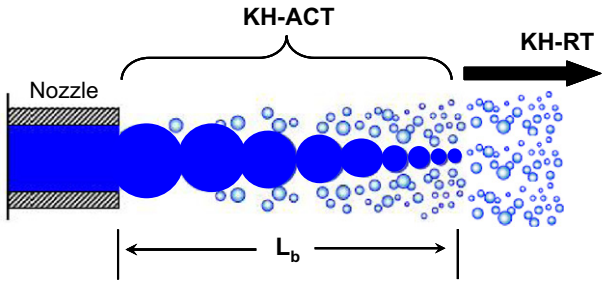


**Fig. 3.** Operation regime of the KH-ACT and KH-RT breakup models. The "breakup length" is also demarcated.

The blob injection model injects liquid drops with a diameter equal to an effective nozzle diameter calculated on the basis of inner nozzle flow simulations. Following injection, the liquid breakup is simulated using primary (KH-ACT) and secondary (KH-RT) breakup models. Details of the KH-ACT primary breakup model and "quasi-dynamic" coupling developed by our group are provided in Refs. [20–23]. The KH-ACT model captures the effects of cavitation and turbulence on primary breakup, in addition to aerodynamic breakup. The KH and RT (Rayleigh–Taylor) models are used to predict the subsequent secondary droplet breakup [29,30]. A breakup length [31] is considered with an intact core length of $L_b$. Within this length, the KH-ACT model is employed, while the KH and RT models compete to cause the droplet breakup outside the core (see Fig. 3).

In the droplet breakup model, it is assumed that the radius of newly formed droplets is proportional to the wavelength of the fastest growing unstable surface wave on the parent droplet. Mass is accumulated from the parent droplet until the shed mass is equal to 5% of the initial parcel mass; at this time, a new parcel is created. Except for the radius, velocity, and number of droplets, the new parcel is given the same properties as the parent parcel. The new parcel is given a component of velocity randomly selected in the plane orthogonal to the direction of the parent parcel. The momentum of the parent parcel is adjusted so that momentum is conserved. The velocity magnitude of the new parcel is the same as the parent parcel.

Droplet collisions are based on the NTC (No Time Counter) algorithm [32]. The computational cost in this model scales linearly with the number of parcels injected (Np), whereas it scales with the square of Np in the O'Rourke collision model [33]. Once collision occurs, the outcomes of the collision are predicted as bouncing, stretching, reflexive separation, or coalescence [34]. A single-component droplet evaporation model [33] based on the Frossling correlation is used. A dynamic drag model is used that postulates that the drag coefficient depends on the shape of the droplet, which can vary between a sphere and a disk. An initially spherical droplet distorts significantly when the Weber number is large. The drag coefficient for a disk is significantly higher than that for a sphere. This dynamic drag model accounts for the effects of drop distortion, varying linearly between the drag of a sphere and a disk [35]. The effects of turbulence on the droplet are also included, using a turbulent dispersion model [33].

## 3. Results and discussion

Our first set of simulations focuses on the injector flow characteristics for biodiesel and diesel fuels. This is followed by results concerning the atomization and spray characteristics of the two fuels under diesel engine conditions. Table 1 presents the physical properties of diesel and biodiesel. An accurate determination of fuel properties is important for reliable prediction of atomization

**Table 1**
Comparison of physical properties of diesel and soy-biodiesel.

| Fuel property | Diesel | Biodiesel |
|---|---|---|
| Carbon content (wt.%) | 87 | 76.74 |
| Hydrogen content (wt.%) | 13 | 12.01 |
| Oxygen content (wt.%) | 0 | 11.25 |
| Density @ 15 °C (kg/m$^3$) | 822.7 | 877.2 |
| Dynamic viscosity @ 40 °C (cP) | 1.69 | 5.626 |
| Surface tension @ 25 °C (N/m) | 0.0020 | 0.00296 |
| Vapor pressure @ 25 °C (Pa) | 1000 | 1 |

and spray processes. Fuel properties reported by Ra et al. [16] for a biodiesel surrogate, methyl butanoate, are used in the present study. The methodology for the calculation of liquid- and vapor-phase physical properties is presented by Chakravarthy et al. [13]. The experimental data from Higgins et al. [12] were obtained for soy-biodiesel, which mainly consists of five methyl esters: methyl palmitate, methyl stearate, methyl oleate, methyl linoleate, and methyl linolenate. The choice of methyl butanoate as surrogate for soy-biodiesel is justified because the physical properties and chemical structure of soy-biodiesel components are similar to those of methyl butanoate. In addition, combustion modeling using detailed chemistry is not feasible with methyl palmitate due to its long alkyl chain. In contrast, with methyl butanoate, the alkyl chain is short enough to develop suitable mechanisms [15] that can be used with reasonable computational costs.

### 3.1. Injector flow simulations

As mentioned earlier, 3-D simulations are performed for flow in a 60°-sector of a production mini-sac nozzle (cf. Figs. 1 and 2) using FLUENT v6.3. A 3-D 60°-sector mesh using 60,000 cells, with tetrahedral elements in the sac region and structured orthogonal grids in other regions was generated. Details of the two-phase models used in these simulations, grid-independence aspect, and validation results using data from Argonne National Laboratory and Winklhofer et al. [36] have been reported in our previous studies [23,26].

Fig. 4 presents the vapor volume fraction ($f_v$) contours for diesel and biodiesel for $P_{inj}$ = 1300 bar and $P_{back}$ = 30 bar at peak needle-lift position. Three different views are shown. The 3-D view of the cavitation contours indicates that vapor generation occurs at the orifice inlet for both fuels. For diesel, these cavitation contours, generated at the upper side of the orifice, reach the orifice exit. In contrast, for biodiesel, the cavitation contours only extend a few microns into the orifice and do not reach the injector exit. The other two views (i.e., a 2-D cut though the mid-plane and a zoomed view of the orifice region) also indicate that the amount of cavitation is significantly reduced for biodiesel compared to diesel. This can primarily be attributed to the low vapor pressure of biodiesel compared with that of diesel (cf. Table 1). Since cavitation plays a significant role in primary breakup, the atomization and spray behavior of these fuels is expected to be different.

The cavitation inception behavior of the two fuels is further examined by plotting the contours of $\frac{d\alpha_v}{dx}$ in Fig. 5, which shows a zoomed 3-D view of the sac and upper orifice region. Here, '$x$' is the coordinate along the orifice axis, and $\alpha_v$ is the vapor mass fraction, related to vapor volume fraction through $\alpha_v = (\rho/\rho_v)\cdot f_v$, with $\rho$ and $\rho_v$ being the mixture and vapor densities, respectively. The parameter $\frac{d\alpha_v}{dx}$ is used as a measure of the production or consumption rate of fuel vapor, with positive and negative values, respectively, representing production and consumption. For both fuels, the sac region contains pure liquid, and thus $\frac{d\alpha_v}{dx} = 0$. The contours indicate that for both fuels, the cavitation (vapor generation) is initiated at the upper side of the orifice inlet. However, the cavitation process along the orifice is significantly different for the two fuels. For diesel, it is characterized by continuous vapor generation, consumption (condensation), and convection; for biodiesel, the vapor is generated at the orifice inlet but is completely consumed soon after in the orifice, with only liquid fuel reaching the injector exit.

Fig. 6 presents contours of the magnitude of velocity at the mid-plane and orifice exit plane for diesel and biodiesel fuels for the case presented in Fig. 4. In addition, average turbulence and cavitation levels at nozzle exit, plus injection and ambient conditions for diesel and biodiesel, are also tabulated in Table 2. The flow entering the orifice encounters a sharp bend (i.e., large velocity and pressure gradients) at the upper side of the orifice inlet, causing cavitation in this region, as indicated by the vapor fraction and $\frac{d\alpha_v}{dx}$ contours in Figs. 4 and 5, respectively. Upstream of the orifice, the velocity distribution appears to be similar for the two fuels. However, at the orifice exit, the contours indicate regions of higher velocity for diesel compared to biodiesel. This is related to the fact that both the molecular and turbulent viscosity (cf. Table 2) of biodiesel are higher than those of diesel. In fact, the molecular

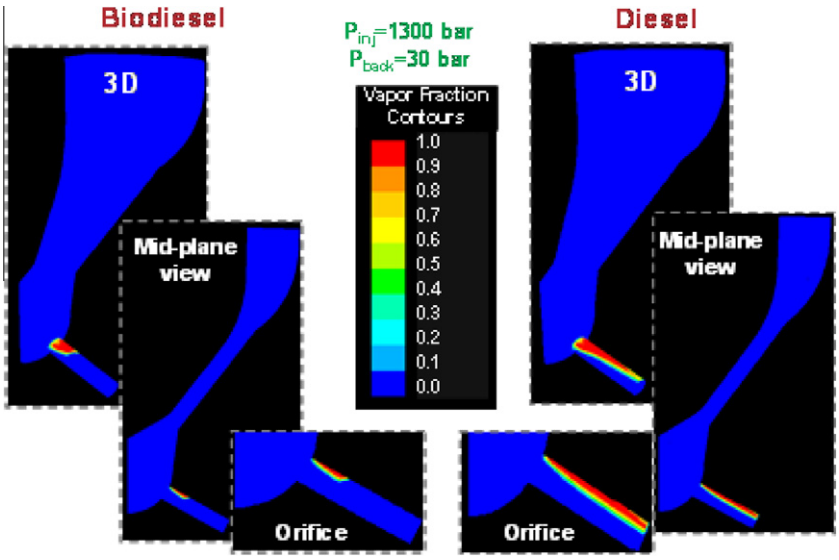


**Fig. 4.** Vapor fraction contours for diesel and biodiesel inside the injector, at the mid-plane and orifice. The simulations were performed at full needle open position with $P_{inj}$ = 1300 bar and $P_{back}$ = 30 bar.

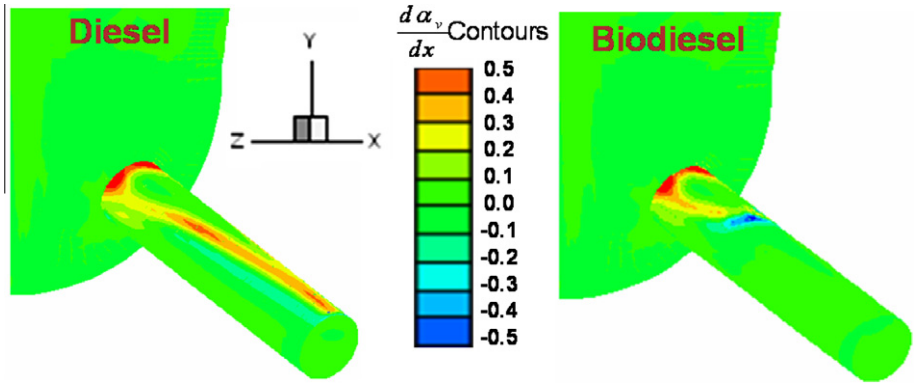


**Fig. 5.** Contours of $\frac{d\alpha_v}{dx}$ for diesel and biodiesel fuels in the sac and orifice regions for the case discussed in the context of Fig. 4.

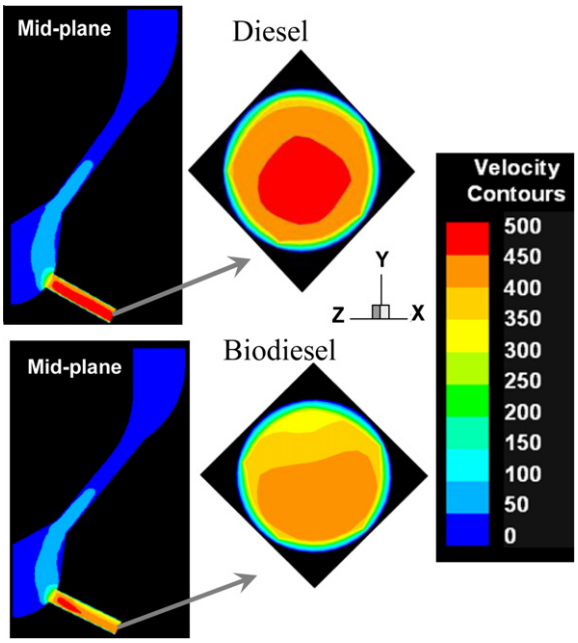


**Fig. 6.** Velocity contours at mid-plane and orifice exit for diesel and biodiesel fuels for the case discussed in the context of Figs. 4 and 5.

**Table 2**
Conditions for diesel and biodiesel for non-evaporating spray simulations.

| Property | Diesel | Biodiesel |
|---|---|---|
| Injection pressure (bar) | 1100/1300 | 1100/1300 |
| Total mass injected (mg) | 17.54/20.94 | 17.18/20.50 |
| Discharge coefficient ($C_d$) | 0.64/0.64 | 0.61/0.62 |
| Area coefficient ($C_a$) | 0.92/0.92 | 1/1 |
| TKE ($m^2/s^2$) | 1409/2410 | 1356/2135 |
| TDR ($m^2/s^3$) | 2.51e + 9/4.23e + 9 | 2.08e + 9/3.24e + 9 |
| Turbulent viscosity (N s/$m^2$) | 0.65/1.13 | 0.78/1.24 |
| Injection duration (ms) | 3 | 3 |
| Ambient density (kg/$m^3$) | 34 | 34 |
| Ambient temperature (K) | 300 | 300 |

viscosity of biodiesel (6.94 cP) is more than 3× higher than that of diesel (2.12 cP) at 300 K (see Table 3). The velocity contours at the orifice exit indicate fairly symmetrical distribution with respect to the *y*-axis for both fuels. (Note that the fuel injection velocity at the orifice exit represents an important parameter for the two-phase flow in the combustor chamber, and therefore, a critical input for the spray breakup and drag models. This aspect and the quasi-dynamic coupling between injector flow and spray simulations are discussed next.)

**Table 3**
Physical properties of biodiesel at different temperatures [15] and of diesel at 300 K.

| Fuel | Injection temperature (K) | Dynamic viscosity (N s/$m^2$) | Density (kg/$m^3$) |
|---|---|---|---|
| Biodiesel | 300 | 0.00694 | 877.2 |
| | 320 | 0.00527 | 871 |
| | 340 | 0.00380 | 860 |
| | 360 | 0.00261 | 846 |
| Diesel | 300 | 0.00212 | 822.7 |

### 3.2. Coupling of injector flow and spray simulations

Fig. 7 presents the computed fuel injection velocity, mass flow rate, discharge coefficient ($C_d$), and normalized turbulent kinetic energy (TKE) [23,26] at the nozzle exit for different injection pressures. All of these parameters are obtained by computing the 3-D flow inside the injector and then averaging the properties at the orifice exit. As expected, with increased injection pressure, the injection velocity and mass flow rate at the orifice exit increase (cf. Fig. 7a). However, the injection velocity, mass flow rate, and discharge coefficient (cf. Figs. 7a and b) are lower for biodiesel compared with those for diesel. This difference in injection velocity, and hence, in mass flow rate, can be attributed to the significantly higher viscosity of biodiesel (cf. Fig. 6). The lower mass flow rate for biodiesel implies that, for a fixed injection duration, a lesser amount of biodiesel will be injected into the combustion chamber compared to diesel. Combined with the lower heating value of biodiesel, this would lead to lower engine output using biodiesel compared to that using diesel. As indicated in Fig. 7b, the averaged turbulence kinetic energy at the nozzle exit is also lower for biodiesel, related to the fact that the Reynolds number is lower for biodiesel due to its higher effective viscosity, as indicated in the context of Fig. 6. This has implications for the atomization and spray characteristics of the two fuels, because the turbulence level at the orifice exit influences the primary breakup.

The preceding discussion indicates that under identical conditions, the mass flow rate is lower for biodiesel compared to diesel, which also implies lower engine output for biodiesel. To address this issue, a parametric study was performed to identify an optimal parameter that can be controlled in order to overcome the loss of engine output associated with the use of biodiesel. The results indicate that decreasing the fuel viscosity by increasing the fuel temperature (cf. Table 3) makes it possible to compensate for the decrease in the biodiesel flow rate. Fig. 8 presents results from

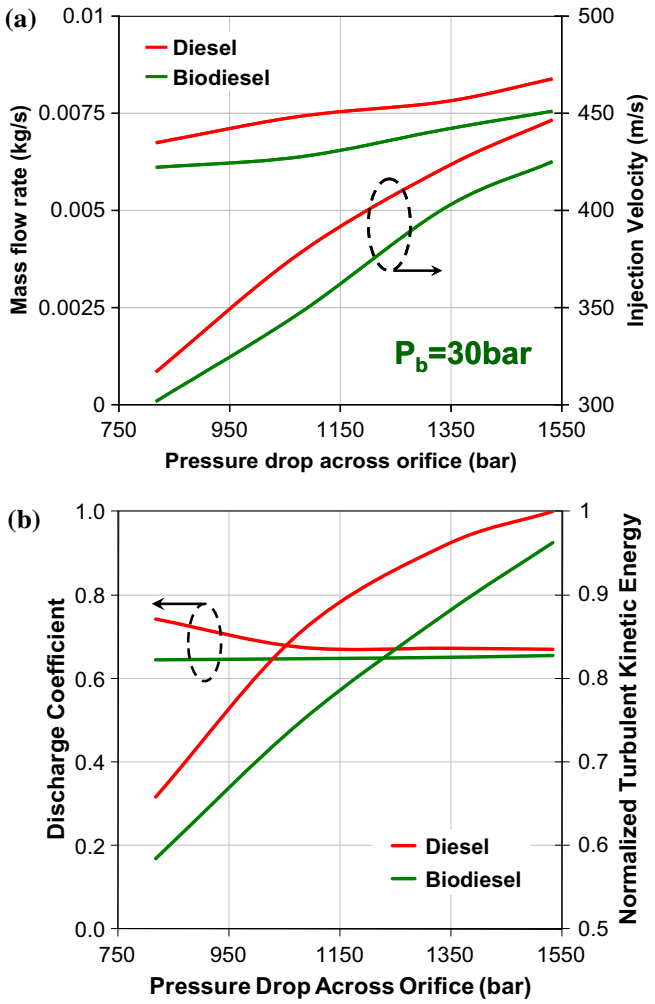


**Fig. 7.** Computed flow properties at the nozzle exit versus pressure drop in the injector for diesel and biodiesel fuels: (a) mass flow rate and injection velocity; (b) discharge coefficient and normalized turbulent kinetic energy.

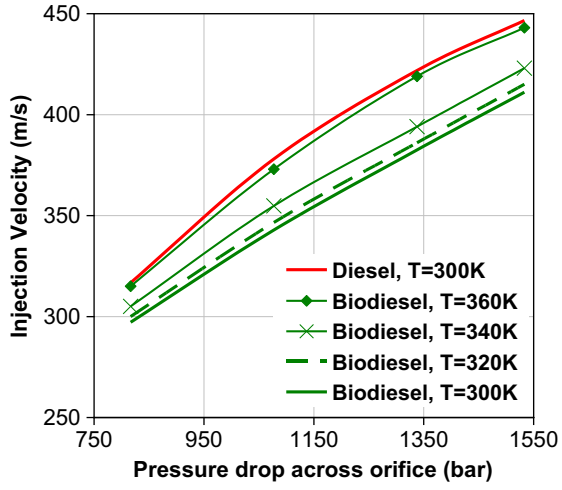


**Fig. 8.** Injection velocity versus pressure drop across the orifice for biodiesel at different injection temperatures and for diesel at an injection temperature of 300 K.

the simulations performed at different biodiesel fuel temperatures. The averaged injection velocity at the orifice exit is plotted for biodiesel fuel at 300, 320, 340, and 360 K and for diesel fuel at 300 K. As the fuel temperature increases, the injection velocity and mass flow rate (not shown here) for biodiesel increase. A fuel temperature of 360 K provides nearly the same injection velocity for biodiesel as that for diesel at 300 K, at all injection pressures. It is important to note, however, that higher fuel temperature may result in higher flame temperature and, thus, increased $NO_x$ emissions.

In order to couple the injector flow and spray simulations, the rate of injection (ROI) profile was computed from injector flow simulations for a common-rail injection system, with the needle fully open during 80% of the injection duration. Fig. 9 presents the computed ROI, as well as the temporal variation of turbulence and cavitation levels (in terms of area coefficient, $C_a$) at the orifice exit during the injection period. These data were subsequently used for spray simulations using CONVERGE, which are discussed in the next section. Consistent with the results discussed earlier in the context of Fig. 7, the fuel flow rate is lower for biodiesel compared with that for diesel. The $C_a$ plot in Fig. 9a indicates significant cavitation at the orifice exit for diesel [26], but no cavitation for biodiesel (i.e., $C_a = 1$). The turbulent kinetic energy plot (cf. Fig. 9b) indicates that the turbulence level for biodiesel is about 12–14% lower compared with that for diesel. Since turbulence and cavitation play a significant role in spray breakup processes,

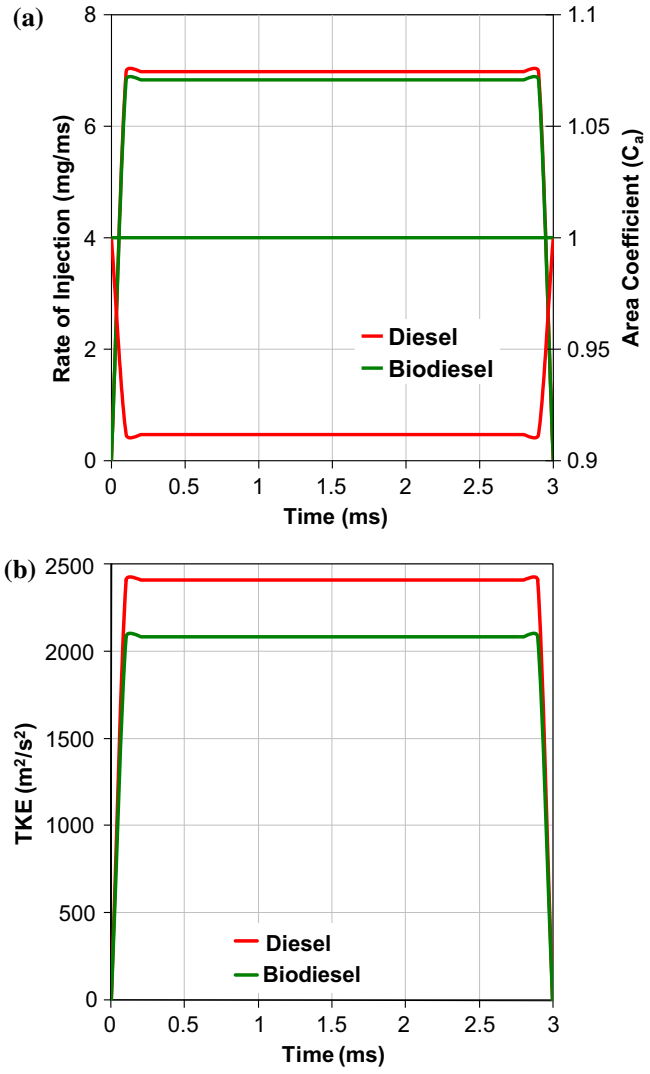


**Fig. 9.** (a) Rate of injection profile, area coefficient; and (b) turbulent kinetic energy at the orifice exit plotted versus time for diesel and biodiesel fuels.

the implication is that the atomization and spray characteristics of biodiesel and diesel fuels may be significantly different. These aspects, for both non-evaporating and evaporating sprays, are discussed next.

### 3.3. Non-evaporating sprays

Results in the preceding section indicate that differences in the physical properties of diesel and biodiesel significantly influence the inner nozzle flow characteristics, including mass flow rate, discharge coefficient, cavitation, and turbulence. This implies that there may also be noticeable differences in their spray characteristics. In this section, we examine this aspect for non-evaporating sprays. Unsteady 3-D simulations were performed for injection in a constant-volume cylindrical chamber (100 mm × 30 mm in axial and radial directions, respectively) at a fixed back pressure of 30 bar and injection pressures of 1100 and 1300 bar. These conditions correspond to those used in X-ray experiments at Argonne [37]. The KH-ACT model was employed to capture the effects of injector flow characteristics' dynamics on the spray behavior. Important parameters for these simulations, including mass of fuel injected, quasi-steady discharge coefficient, area coefficient, turbulent kinetic energy, and turbulence dissipation rate, are listed in Table 2. As indicated, the ambient conditions and injection temperature were kept the same for the two fuels.

Fig. 10 shows the computed spray structures in terms of droplet sizes at different times (0.5, 1.0, 1.5, and 2.0 ms) from SOI for diesel and biodiesel fuels. The black vertical line near the spray tip in each plot indicates the maximum penetration. The injection pressure is 1100 bar. The global spray structures for the two fuels appear to be similar, but there are noticeable quantitative differences in terms of spray penetration, dispersion, cone angle, etc., as discussed below.

Fig. 11 presents the spray penetration versus time for the two fuels at two different injection pressures. Predictions are shown for both the KH and KH-ACT models. Grimaldi et al. [3] observed that the spray penetration is larger, while the cone angle is smaller, for biodiesel compared to diesel. As indicated in Fig. 11, the KH-ACT model captures this experimental trend accurately (i.e., larger spray penetration for biodiesel compared with that for diesel). In contrast, the KH model predicts smaller penetration for biodiesel compared with that for diesel. The cavitation and turbulence generated inside the nozzle are known to destabilize the jet, which promotes atomization, leading to smaller droplets, and

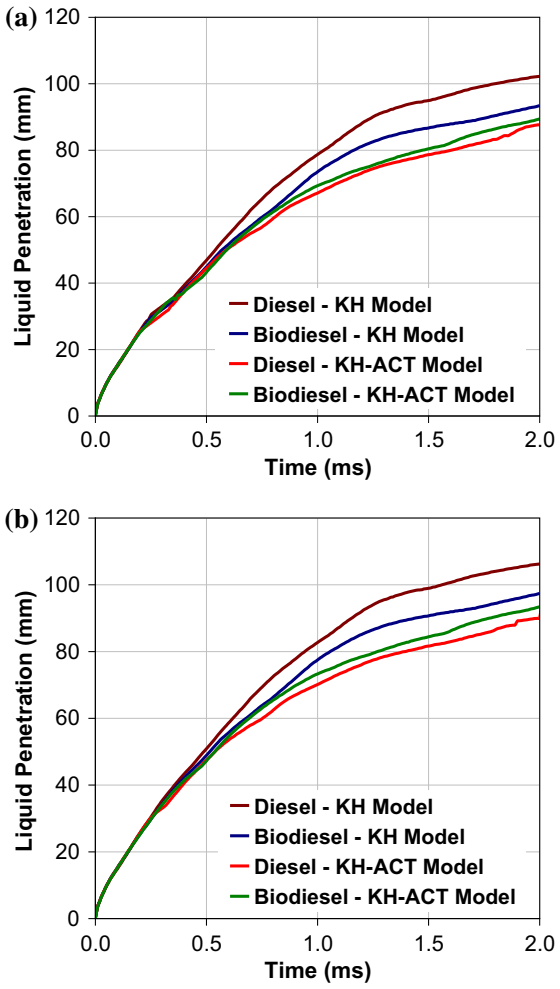


**Fig. 11.** Predicted spray penetration versus time (from SOI) for diesel and biodiesel fuels using KH and KH-ACT models at injection pressure of: (a) 1100 bar and (b) 1300 bar.

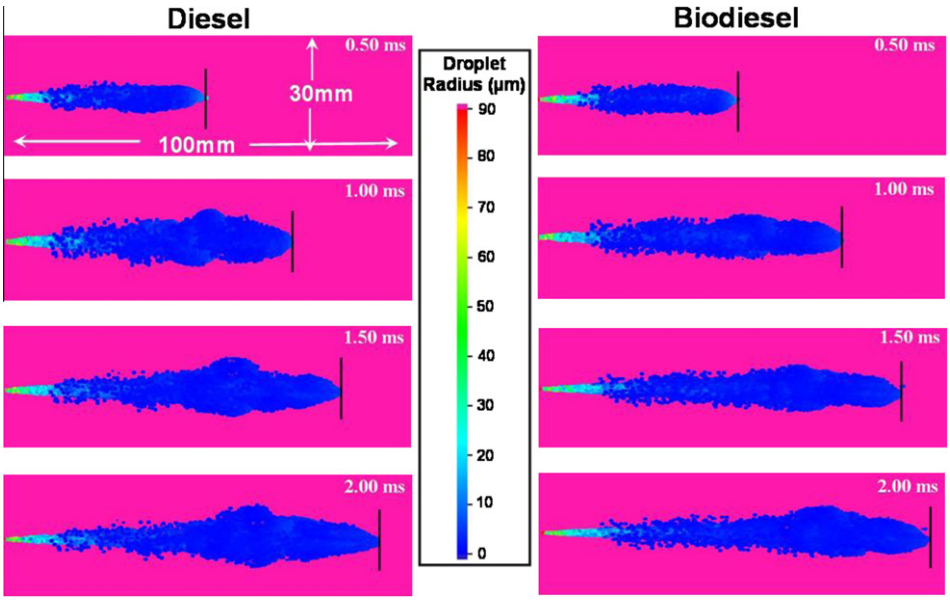


**Fig. 10.** Computed spray structure at different times from SOI for diesel and biodiesel. The droplet size contours are also shown. *P*inj = 1100 bar and *P*back = 30 bar.

hence, smaller spray penetration. These inner nozzle flow effects are not captured by the KH model, which only considers aerodynamically induced breakup. On the other hand, the KH-ACT model captures the effects of reduced cavitation and turbulence levels, predicting higher spray penetration for biodiesel.

Fig. 12 presents additional results characterizing differences in the atomization behavior of the two fuels, in terms of the temporal variation of Sauter mean diameter (SMD) and number of excess parcels. The number of excess parcels represents the additional number of parcels created due to breakup by inner nozzle flow effects, or the difference between the number of parcels predicted by KH-ACT and KH models. The slower breakup process for biodiesel is readily seen by the larger SMD, especially after 0.2 ms from start of injection (SOI), and by the smaller number of excess parcels. As mentioned earlier, the slower primary breakup results from the suppression of cavitation and turbulence for biodiesel.

It is interesting to note that the fuel physical properties have a more pronounced effect on the inner nozzle flow than they have on the spray characteristics. For instance, the discharge coefficient, injection velocity, and TKE were lower by 7–8%, 8–10%, and 12–14%, respectively, for biodiesel compared with those for diesel (cf. Figs. 7b and 9). However, the spray penetration predicted using the KH-ACT model is only 2–3% higher for biodiesel, although it is consistent with the experimental trends [3]. Spray penetration is characterized by two competing effects. Enhanced spray breakup typically results in smaller SMD and thus reduced spray penetration, whereas the increased fuel flow rate (ROI) increases injection velocity which leads to an increase in spray penetration. For petrodiesel, it should be noted that cavitation, TKE, and injection velocities are higher (cf. Figs. 4 and 7). Higher TKE and cavitation result in enhanced spray breakup for petrodiesel. However, due to its higher ROI, the differences in spray characteristics are small yet significant. It is also important to note that the KH model predicts a difference of about 10% in spray penetration; however, it fails to capture the experimental trends reported in the literature [3]. Since the KH-ACT model accurately captures the experimental trends, the following results are presented only for this latter model.

Fig. 13 presents the near-field ($x_1$ = 2.5 mm) and far-field ($x_2$) spray dispersion for the two fuels. The near-field dispersion (cf. Fig. 13a) is represented in terms of the projected mass density plots [20,23,37]. The projected mass density has a Gaussian distribution for both fuels, with the tail representing the extent of spreading or dispersion. In order to provide a perspective on the extent of spreading, the nozzle diameter is indicated by a small black box in Fig. 13a. The far-field spray dispersion (cf. Fig. 13b) is characterized in terms of the full cone angle measured at 60% of peak penetration ($S$) at a given time (i.e., at $x_2$). The near-field spray dispersion characteristics are nearly similar for the two fuels, with marginally higher dispersion for diesel. The differences become more pronounced in the far-field region, as the cone angle for diesel is about 2° higher than that for biodiesel. This is consistent with the results concerning spray penetration and SMD for the two fuels, presented in Figs. 10–12.

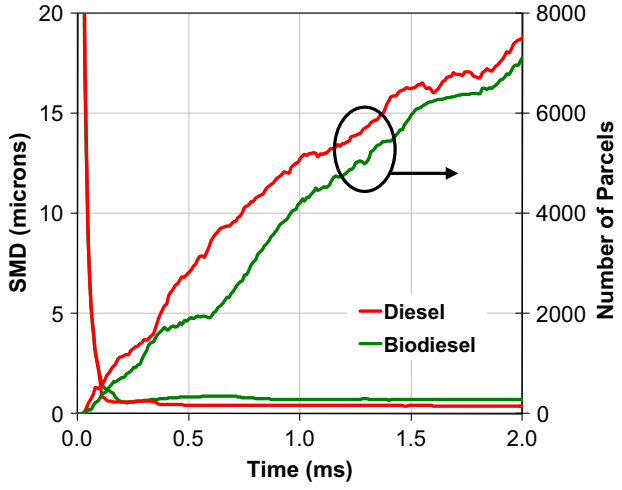


**Fig. 12.** SMD and number of excess parcels versus time for diesel and biodiesel for the case presented in context of Fig. 11 for an injection pressure of 1100 bar.

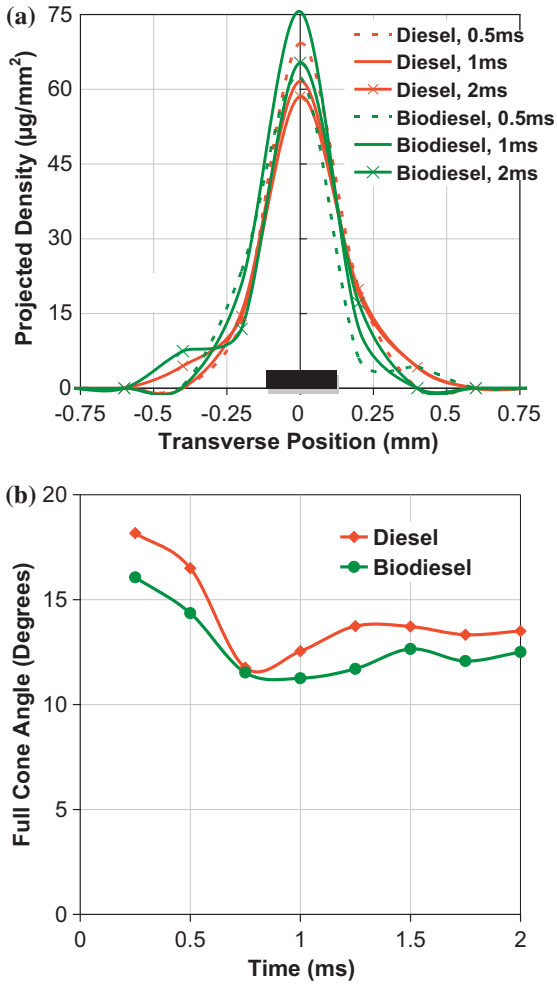


**Fig. 13.** (a) Projected mass density distribution in the transverse direction at different times after SOI; the axial location is $x$ = 2.5 mm (near field). (b) Spray cone angle at $x_2$ (far field) versus time for diesel and biodiesel fuels.

In summary, results for non-evaporating sprays indicate that the suppression of cavitation and turbulence for biodiesel leads to greater spray penetration, larger SMD, smaller dispersion, and smaller cone angle for this fuel compared with those for diesel.

### 3.4. Evaporating sprays

Simulations for evaporating sprays were performed corresponding to experimental conditions (see Table 4) used by Higgins et al. [12], who conducted experiments for several fuels, including diesel, Fischer–Tropsch diesel, fatty acid methyl ester (FAME) biodiesel, unleaded gasoline, methanol, n-hexadecane, and heptamethylnonane. In the absence of geometrical details for the nozzle orifice used at Sandia National Laboratory, empirical correlations were used to determine the TKE, TDR, and extent of cavitation, as

**Table 4**
Range of conditions for evaporating spray experiments performed by Higgins et al. [12].

| Parameter | Quantity |
|---|---|
| Injection system | Detroit diesel, common rail |
| Number of orifices | 1 – Cylindrical, non-hydroground |
| Orifice diameter | 100 to 500 urn, $L/D = 4.2$ |
| Injection pressure (bar) | 400 to 1900 |
| Chamber density (kg/m$^3$) | 3.3 to 60 |
| Chamber temperature (K) | 700 to 1300 |
| Fuel temperature (K) | 375 to 440 |
| Measured discharge coefficient | 0.78 to 0.84 |

done in our previous study [20]. Since the ROI is typically a top-hat profile, these values at peak needle-lift position were used for evaporating spray simulations. As shown in our previous study [20], with such an approach, liquid length and vapor penetration can be accurately captured.

Fig. 14 presents a comparison of the measured and predicted spray structures for diesel and biodiesel at an ambient temperature of 1000 K, ambient density of 14.8 kg/m$^3$, orifice diameter of 246 μm, injection pressure of 142 MPa (cf. Table 4), and an injection duration of 5 ms. Simulations were performed with the KH-ACT primary breakup model, using the same model constants for the two fuels as were used for the non-evaporating spray studies presented earlier. In simulations, n-heptane and methyl butanoate were used as surrogates for the diesel and soy-biodiesel fuel, respectively. The temperature-dependent fuel properties, such as density, kinematic viscosity, surface tension, vapor pressure, heat of vaporization, and specific heat, were obtained from Ra et al. [16]. Note that only very limited data are available for the properties of various biodiesels. The measured spray structure is presented in terms of the superimposed Mie and Schlieren images, while the predicted structure is in terms of the droplet parcels' locations during the quasi-steady period (i.e., at 1.5 ms from SOI). The field of view in the axial and radial directions is 50 and 15 mm, respectively. The predictions reproduce the experimental trend in terms of the higher liquid penetration for biodiesel compared to diesel. However there are noticeable differences between the predicted and measured liquid lengths for biodiesel, the liquid length being underpredicted by about 6 mm. This can be attributed to (i) differences in the fuel properties, especially the boiling temperature and heat of vaporization, (ii) deficiency in the evaporating model used, and (iii) determination of liquid length from simulations which are based on 97% of the encompassed liquid fuel mass. Further studies will be performed to improve the liquid length predictions for biodiesel. Based on the available experimental data regarding liquid length and simulation results for non-evaporating sprays, it seems that spray behavior is more strongly influenced by vaporization properties, such as heat of vaporization and $T_{90}$, compared to other fuel physical properties such as density, viscosity, and surface tension.

Fig. 15 presents the predicted and measured liquid lengths versus ambient temperature for diesel and biodiesel fuels. Other conditions were the same as those for the results presented in Fig. 14. As the ambient temperature is increased, the liquid length decreases due to the enhanced vaporization rate. There is generally good agreement between predictions and measurements, but the liquid lengths are noticeably underpredicted for biodiesel, which may be attributed to differences in the fuel properties, as mentioned earlier. Fig. 16 presents simulated images characterizing the liquid and vapor penetration with respect to time for the two fuels. The liquid distribution is indicated by plotting the locations of droplet parcels (pink dots), while the vapor structure at different times is shown by (fuel vapor) equivalence ratio contours. The field of view in the axial and radial directions is 50 and 15 mm, respectively. The solid and dashed lines represent liquid and vapor penetration lengths, respectively. As the injection starts, the liquid length increases with time and stabilizes at ~0.5 ms after SOI. The vapor penetration, however, continues to increase as the evaporated fuel vapor is convected downstream. In addition, the equivalence ratio decreases downstream due to air–fuel mixing. Although the global liquid and vapor penetration characteristics for the two fuels are similar, both the liquid length and vapor penetration are higher for biodiesel compared with those for diesel. This is an important result, because once the liquid length is stabilized, the vapor penetration determines the fuel–air mixing and thereby the combustion and emission characteristics.

An important observation from the above results is that, for evaporating sprays under identical injection and ambient conditions, the liquid length for biodiesel is noticeably higher than that for diesel. This could have important implications for running the same diesel engine with biodiesel, since the use of biodiesel may

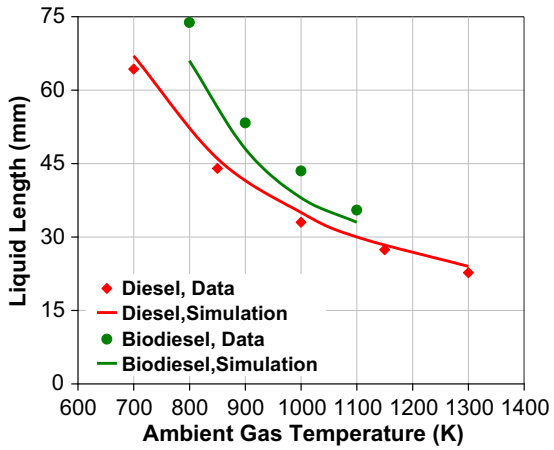


**Fig. 15.** Measured and predicted liquid lengths versus ambient gas temperature for diesel and biodiesel fuels for conditions specified in Table 4.

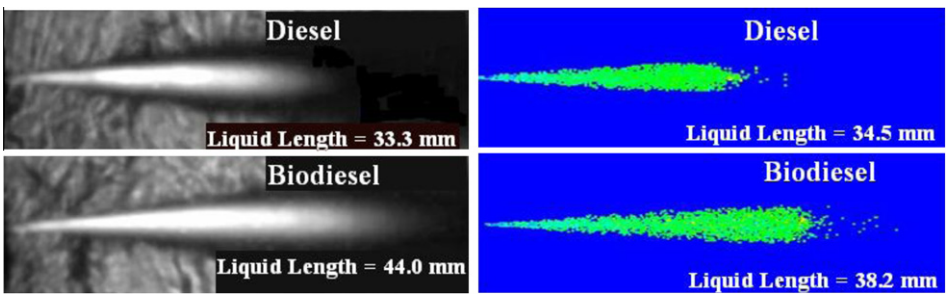


**Fig. 14.** Measured and predicted spray structures for diesel and biodiesel at an ambient temperature of 1000 K.

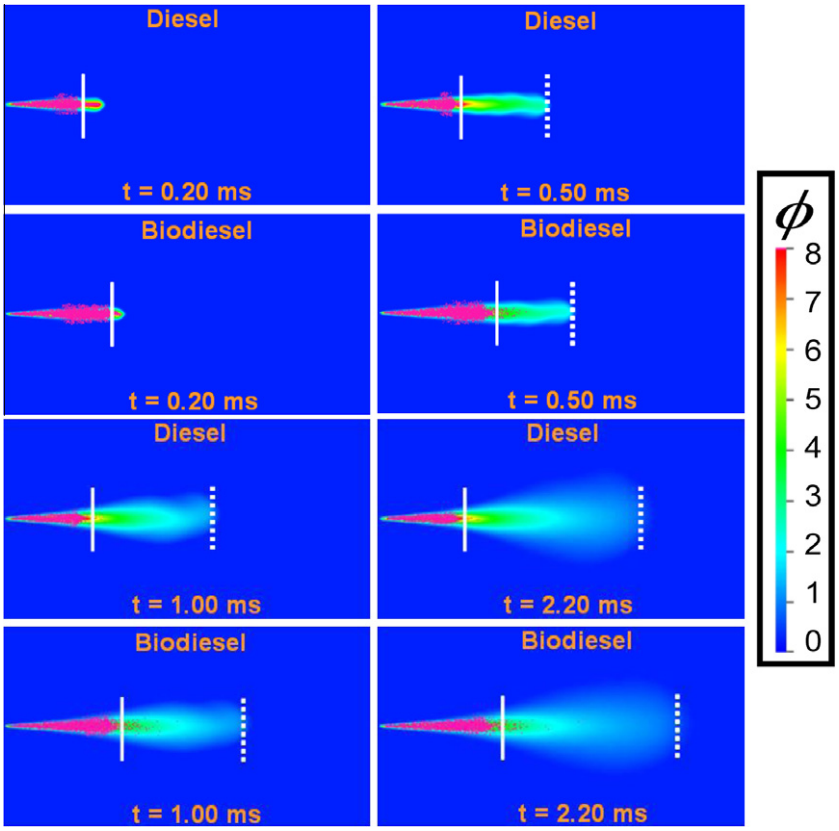


**Fig. 16.** Liquid penetration and equivalence ratio (based on fuel vapor) contours for diesel and biodiesel fuels at different times from SOI for the cases discussed in the context of Fig. 14.

require changes in the piston bowl design or in the injection and/or ambient conditions in order to ensure similar liquid lengths for the two fuels. With respect to the latter, it may be easier to control the ambient gas density, fuel injection pressure, and temperature. For instance, our simulations indicate that increasing the ambient density by about 30% would yield a liquid length for biodiesel similar to that for diesel. While further parametric studies are necessary to quantitatively determine the necessary changes in engine parameters, our simulations indicate that, for a fixed compression ratio engine, the ambient density (i.e., air-intake pressure) and/or fuel injection temperature need to be higher for biodiesel to ensure similar liquid lengths for the two fuels.

## 4. Conclusions

A computational study was performed to investigate the injection and spray behavior of biodiesel and diesel fuels. Detailed 3-D injector flow simulations were performed using FLUENT v6.3, while spray simulations were performed using an engine modeling software, CONVERGE. The two sets of simulations were coupled through a recently developed KH-ACT model that accounts for the effects of cavitation and turbulence, in addition to aerodynamic effects, on the primary liquid breakup. Important observations are as follows:

(1) There are significant differences between the injector flow characteristics of biodiesel and diesel fuels. In particular, the cavitation and turbulence levels are significantly lower for biodiesel compared with those for diesel, and this can be attributed to the lower vapor pressure of biodiesel. In addition, the injection velocity, discharge coefficient, and mass flow rate are lower for biodiesel, due to its higher viscosity. In order to account for the viscous losses, biodiesel would need to be injected at about 60 K higher temperature compared to diesel.
(2) Biodiesel exhibits poor atomization characteristics compared to diesel; the spray penetration and SMD are higher, while dispersion and cone angle are smaller, for biodiesel, consistent with experimental trends reported in literature. These experimental trends could not be accurately captured by the KH model, but they were captured by the KH-ACT model, thus demonstrating the effectiveness of the latter in capturing the primary breakup phenomenon.
(3) The predicted liquid length and vapor penetration are higher for biodiesel compared to diesel, which is also consistent with measurements reported in the literature. However, simulations generally underpredict the liquid length compared to actual measurements; this is mainly attributed to the underprediction of vaporization rates due to a lack of accurate information on biodiesel fuel properties, including boiling temperature and heat of vaporization.
(4) Differences in the spray characteristics of biodiesel and diesel fuels are more pronounced for evaporating sprays compared to those for non-evaporating sprays. This is due to the higher boiling temperature and higher heat of vaporization of biodiesel, implying that vaporization properties rather than fuel physical properties, such as density, viscosity, and surface tension, have a more significant influence on spray behavior.
(5) An important conclusion from the present study is that differences in the injection and spray behavior of the two fuels may require changes in the piston bowl design or in the injection and/or ambient conditions in order to use biodiesel in an existing diesel engine. The present simulations suggest

that fuel injection temperature and ambient density may be the two parameters that can be controlled.

## Acknowledgments

The submitted manuscript has been created by UChicago Argonne, LLC, Operator of Argonne National Laboratory (“Argonne”). Argonne, a US Department of Energy Office of Science laboratory, is operated under Contract No. DE-AC02-06CH11357. The US Government retains for itself, and others acting on its behalf, a paid-up nonexclusive, irrevocable worldwide license in said article to reproduce, prepare derivative works, distribute copies to the public, and perform publicly and display publicly, by or on behalf of the Government.

## References

[1] Graboski MS, McCormick RL. Combustion of fat and vegetable oil derived fuels in diesel engines. Progress in Energy and Combustion Science 1998;24:125–64.
[2] Armas O, Hernandez J, Cardenas M. Reduction of diesel smoke opacity from vegetable oil methyl esters during transient operation. Fuel 2006;85:2427–38.
[3] Grimaldi CN, Postrioti L, Battistoni M, Millo F. Common rail HSDI diesel engine combustion and emissions with fossil/bio-derived fuel blends. SAE Paper No. 2002-01-0865; 2002.
[4] Hashimoto M, Dan T, Asano I, Arakawa T. Combustion of the rape-seed oil in a diesel engine. SAE Paper No. 2002-01-0865; 2002.
[5] Agarwal AK. Performance evaluation and tribological studies on a biodiesel fuelled compression ignition engine. PhD thesis, Indian Institute of Technology (Delhi); 1999.
[6] Miers SA, Kastengren AL, El-Hannouny EM, Longman DE. An experimental investigation of biodiesel injection characteristics using a light-duty diesel injector. ASME ICEF 2007-1735; 2007.
[7] Suh HK, Park SH, Lee CS. Experimental investigation of nozzle cavitating flow characteristics for diesel and biodiesel fuels. International Journal of Automotive Technology 2008;9:217–24.
[8] Park SH, Suh HK, Lee CS. Effect of cavitating flow on the flow and fuel atomization characteristics of biodiesel and diesel fuels. Energy and Fuels 2008;22:605–13.
[9] Kastengren AL, Powell CF, Im KS, Wang YJ, Wang J. Measurement of biodiesel blend and conventional diesel spray structure using X-ray radiography. ASME ICES 2008-1646; 2008.
[10] Rotondi R, Bella G, Grimaldi CN, Postrioti L. Atomization of high pressure diesel spray: experimental validation of a new breakup model. SAE Paper No. 2001-01-1070; 2001.
[11] Postrioti L, Grimaldi CN, Ceccobello M, Gioia R. Diesel Common rail injection system behavior with different fuels. SAE Paper No. 2004-01-0029; 2004.
[12] Higgins BS, Mueller CJ, Siebers DL. Measurements of fuel effects on liquid-phase penetration in DI sprays. SAE Paper No. 1999-01-0519; 1999.
[13] Chakravarthy K, McFarlane J, Daw SC, Ra Y, Reitz RD. Physical properties of soy bio-diesel and implications for use of biodiesel in diesel engines. SAE Paper No. 2007-01-0430; 2007.
[14] Lefebvre AH. Atomization and sprays. Taylor and Francis; 1989.
[15] Brakora JL, Ra Y, Reitz RD, McFarlane J, Law CS. Development and validation of a reduced reaction mechanism of biodiesel-fueled engine simulations. SAE Paper No. 2008-01-1378; 2008.
[16] Ra Y, Reitz RD, McFalane J, Law CS. Effects of fuel physical properties on diesel engine combustion using diesel and bio-diesel fuels. SAE Paper No. 2008-01-1379; 2008.
[17] Senecal PK, Pomraning E, Richards KJ. Multi-dimensional modeling of direct-injection diesel spray liquid length and flame lift-off length using CFD and parallel detailed chemistry. SAE Paper No. 2003-01-0243; 2003.
[18] Senecal PK, Richards KJ, Pomraning E, Yang T, Dai MZ, McDavid RM, et al. A new parallel cut-cell Cartesian CFD code for rapid grid generation applied to in-cylinder diesel engine simulations. SAE Paper No. 2007-01-0159; 2007.
[19] Richards KJ, Senecal PK, Pomraning E. CONVERGE™ (Version 1.2) manual. Middleton, WI: Convergent Science, Inc.; 2008.
[20] Som S, Ramírez AI, Aggarwal SK, Kastengren AL, El-Hannouny EM, Longman DE, et al. Development and validation of a primary breakup model for diesel engine applications. SAE Paper No. 2009-01-0838; 2009.
[21] Som S, Aggarwal SK. Modeling diesel spray flame lift-off using detailed chemistry and a new primary breakup model. 47th AIAA 2009-0666; 2009.
[22] Som S, Aggarwal SK. Effects of primary breakup modeling on spray and combustion characteristics of compression ignition engines. Combustion and Flame 2010;157(6):1179–93.
[23] Som S. Development and validation of spray models for investigating diesel engine combustion and emissions. PhD thesis, University of Illinois at Chicago; 2009.
[24] Som S, Aggarwal SK. An assessment of atomization models for diesel engine simulations. Atomization and Sprays 2009;19(9):885–903.
[25] FLUENT v6.3 documentation.
[26] Som S, Aggarwal SK, El-Hannouny EM, Longman DE. Investigation of nozzle flow and cavitation characteristics in a diesel injector. Journal of Engineering for Gas Turbine and Power 2010;132(4):1–12.
[27] Singhal AK, Athavale AK, Li H, Jiang Y. Mathematical basis and validation of the full cavitation model. Journal of Fluid Engineering 2002;124:617–24.
[28] Brennen EC. Cavitation and bubble dynamics. Oxford University Press; 1995.
[29] Reitz RD. Modeling atomization processes in high pressure vaporizing sprays. Atomization and Spray Technology 1987;3:309–37.
[30] Patterson MA, Reitz RD. Modeling the effects of fuel spray characteristics on diesel engine combustion and emissions. SAE Paper No. 980131; 1998.
[31] Beale JC, Reitz RD. Modeling spray atomization with the Kelvin–Helmholtz/Rayleigh–Taylor hybrid model. Atomization and Sprays 1999;9:623–50.
[32] Schmidt DP, Rutland CJ. A new droplet collision algorithm. Journal of Computational Physics 2000;164:62–80.
[33] Amsden AA, O'Rourke PJ, Butler TD. KIVA-II: a computer program for chemically reactive flows with sprays. Los Alamos National Laboratory Report No. LA-11560-MS; 1989.
[34] Post SL, Abraham J. Modeling the outcome of drop–drop collisions in diesel sprays. International Journal of Multiphase Flow 2002;28:997–1019.
[35] Liu AB, Mather DK, Reitz RD. Modeling the effects of drop drag and breakup on fuel sprays. SAE Paper No. 930072; 1993.
[36] Winklhofer E, Kull E, Kelz E, Morozov A. Comprehensive hydraulic and flow field documentation in model throttle experiments under cavitation conditions. ILASS Europe 2001.
[37] Ramírez AI, Som S, Aggarwal SK, Kastengren AL, El-Hannouny EM, Longman DE, et al. Quantitative X-ray measurement of high-pressure fuel sprays from a production heavy duty diesel injector. Experiments in Fluids 2009;47:119–34.